Nanomed Res J 6(4):409-418, Autumn 2021

RESEARCH ARTICLE

Synthesis and Characterization of Rod-shaped Gold Nanoshell on the Magnetite (Fe_3O_4) Core

Omid Amirizadeh [1, ¥], Milad Fadaie [2, ¥], Mohammad Jafar Molaei [3], Esmaeil Mirzaei [1,4 *]

[1] Department of Medical Nanotechnology, School of Advanced Medical Sciences and Technologies, Shiraz University of Medical Sciences, Shiraz, Iran.

[2] Pharmaceutical Sciences Research Center, Shiraz University of Medical Sciences, Shiraz, Iran.

[3] Faculty of Chemical and Materials Engineering, Shahrood University of Technology, Shahrood, Iran.

[4] Nanomedicine and Nanobiology Research Center, Shiraz University of Medical Sciences, Shiraz, Iran.

¥ Omid Amirizadeh and Milad Fadaie equally contributed to this work as first authors.

ARTICLE INFO

Article History:
Received 12 Aug 2021
Accepted 27 Sep 2021
Published 01 Nov 2021

Keywords:
surface plasmon resonance
rod-shaped
gold nanoshell
magnetite

ABSTRACT

Objective(s): This paper describes the preparation and characterization of rod-shape gold nanoshells over Fe_3O_4 nanorods. This hybrid nanostructure combines plasmonic properties of the gold nanoshells and magnetic behavior of the magnetite nanorods in a single platform which turns it into a promising choice for multi-purpose biomedical applications

Methods: The Fe_3O_4 core was formed via hydrazine reduction of FeOOH rods synthesized through a simple hydrothermal method. The Fe3O4 core was then modified with APTES and underwent gold seeding and plating to form the final nanoshell. The formation of FeOOH and Fe_3O_4 particels were confirmed through x-ray diffraction analysis.

Results: The formed particles showed rode shape morphology based on scanning electron microscopy. The Fe_3O_4/Au (core/shell) particles showed two broad surface plasmon resonance (SPR) absorption peaks around 750 nm and 930 nm. Both SPR peaks are in the transmission window for biological entities (skin, tissue, and hemoglobin).

Conclusions: These combined magnetic and optical properties suggest the rod-shaped gold nanoshell as a proper theranostic agent for biomedical applications.

How to cite this article
Amirizadeh O., FadaieM., Molaei M.J., Mirzaei E. Synthesis and Characterization of Rod-shaped Gold Nanoshell on the Magnetite (Fe_3O_4) Core. Nanomed Res J, 2021; 6(4): 409-418. DOI: 10.22034/nmrj.2021.04.010

INTRODUCTION

The interaction of free conduction electrons of noble metals with the electromagnetic radiation, at the optical range, can lead to an increase in collective oscillations of the charge density which is typically known as "surface plasmon" [1]. In the recent years, a great deal of attention has been attracted to the metallic nanostructures with plasmon tunability due to their potential for being an ideal candidate using in plasmonic photothermal applications [1, 2]. In the case of localized plasmon resonance, as a geometry-dependent feature, changing of size and geometry can finely tune the plasmonic behavior of metallic nanostructures [3-5]. Among metallic nanostructures, nanorods and nanoshells most typically show the size- and geometry-dependent plasmon resonant properties [6-8].

Gold nanostructures provide a great potential for using in extensive biomedical applications owing to their ease of preparation, capability of bio-conjugation, and unique optical properties [9]. Additionally, favorable biocompatibility and tunable photothermal behavior of these nanostructures turns them into an ideal candidate for a wide range of diagnostic and therapeutic

* Corresponding Author Email: *e_mirzaei@sums.ac.ir*

applications (13). To exemplify, rod-shaped gold nanoparticles have been widely utilized in the development of biomolecules detection sensors, targeting drug delivery systems, and laser-based hyperthermia platforms (14).

In general, altering intrinsic features of nanostructures such as size, shape (sphere, rod, or cube), and type of the material, might adjust the plasmon resonance band through a wide spectral range [10]. It is assumed that rod-shaped gold nanostructures represent the strongest surface plasmon enhancement among the other shapes [11]. The electrons oscillation along the longitudinal and transverse axes of gold nanorods makes two tunable plasmon resonances [12]. The longitudinal and transverse plasmon resonance can be regularly tuned by altering the nanorod length and width respectively.

As a general trend, the absorption and scattering wavelength of gold nanostructures is shifted from visible to NIR region by changing the shape from spherical to rod-shaped nanoparticles [13, 14]. From this, Tuning the aspect ratios of rod-shaped gold nanostructures is a routine approach to enable them to absorb and scatter drastically in the near-infrared (NIR) region (680-1100 nm) [15]. It is worth mentioning that, nanostructures with plasmonic absorption at the NIR region are more preferable for in-vivo applications due to their superior functionality within the depth of body tissues [16]. The factor that makes NIR plasmonic nanostructures ideal candidates for a wide variety of diagnostic and therapeutic puposes.

The tunable plasmon resonances of nanoshells correspond to the hybridization of the plasmon at the inner and outer surface of the shell layer with each other. Accordingly, hanging the relative ratio of the inner radius to the outer radius in metallic nanoshells adjust the corresponding plasmon resonances [5, 17].

Gold nanoshells (GNSs) are typically a thin coating layer formed on a core nanoparticle with a low dielectric constant [18]. The thickness of GNSs might be varied in the range of a few to tens of nanometers [19]. Analogues to gold nanorods, GNSs exhibit strong plasmonic absorbance as well as favorable scattering performance [20]. However, a major privilege for gold nanoshells is the strong and tunable extinction they represent in the near-infrared region of the electromagnetic spectrum [21]. Accordingly, utilization of rod-shaped gold nanoshells can be a potentially smart strategy to develop functional in order to real-time imaging simultaneous to localized photothermal therapy. Interestingly, the relative core/shell ratio of these nanocomposites can finely tune their surface plasmon resonance (SPR) over the region of visible to near-infrared spectrum [22-24].

Owing to the unique physicochemical capabilities, magnetic nanoparticles have represented a great potential for using in a wide collection of applications [25]. As a distinctive characteristic, magnetic materials can be easily manipulated in the presence of an external magnetic field. As an illustration, iron oxide-based materials are capable of being separated, concentrated, and/or directed by using an external magnetic field which turns them into the ideal candidates for various biomedical applications such as protein separation, targeted drug delivery, magnetic resonance imaging (MRI), and magnetic hyperthermia [26].

As a rational approach, versatile and multifunctional biomedical platforms can be developed using combined nanoscale materials to take advantage of real-time diagnosis, targeted delivery, and localized hyperthermia, simultaneously [27-29]. Accordingly, when the magnetic nanoparticles are optimally combined with the noble metals in a single monolith platform, a unique multifunctional platform with favorable properties could be represented. For instance, core/shell nanoparticles comprised of a magnetic core and metallic shell, such as Fe_3O_4/Au and Fe_3O_4/Ag nanoparticles, are desirable platfroms for being utilized in theranostic applications [30]. These binary platforms are more stable in corrosive conditions and can be robustly functionalized using thiol-Au interactions. More importantly, the gold coating layer can potentially yielding the system a favorably tunable plasmonic properties [31].

In the present study, we developed a rod-shaped gold nanoshell on a rod-like magnetic core. This hybrid nanostructure combines plasmonic properties of the gold nanoshells and magnetic behavior of the magnetite nanorods in a single platform which turns it into a promising choice for multi-purpose biomedical applications. Inspite of the similar researches, formation of Fe_3O_4 nanorods, as a magnetic core, was aimed to be acquired by a particular synthesis procedure and confirmed through the characterization tests in this study. Additionally, surface coating of the magnetite nanorods with a structurally-optimized gold layer was another distinctive

factor for our study comparing with the similar ones. However, some analogues studies have represented structurally-comparable platforms, their functionalies are majorly not explicit or affiramable. From this, in order to investigate the functionality of our versatile platform, we tried to provid the distinct corresponding results of the examination of core magnetic properties and shell plasmonic characteristic.

MATERIALS AND METHOD

Chemicals

Ferric chloride ($FeCl_3.6H_2O$, 97%), hydrazine (N_2H_4, 98%), potassium carbonate (K_2CO_3, 99%), formaldehyde (2%), 3-aminopropyltriethoxysilane (APTES), sodium hydroxide (NaOH), absolute ethanol, gold (III) chloride tri-hydrate ($AuCl_3.3H_2O$) were used as chemicals in this study. In order to preparation of APTES stock solution, 12 mM APTES was dissolved in absolute ethanol/ water (4:1) mixture. All the chemicals were purchased from Sigma Aldrich (Germany) and utilized without conducting any further purification. Ultra-pure water was used throughout the synthesis process.

Preparation of β-FeOOH and magnetite nanorods

Rod-shaped β-FeOOH nanoparticles were obtained from hydrolysis of $FeCl_3$ aqueous solution according to the method developed by Yue et al [32]. In a typical procedure, $FeCl_3.6H_2O$ was dissolved in 30 ml of deionized water and stirred for 1 h for achieving a homogenous solution with a Fe^{3+} concentration of 0.05 M. Subsequently, the homogeneous $FeCl_3$ solution was transferred into a Teflon-lined stainless steel autoclave. The autoclave was placed into a laboratory oven and heated at 80 °C for 12 h. After cooling down the autoclave to room temperature, the yellow-colored precipitates, formed at the bottom of container, were harvested through centrifugation, rinsed by distilled water, dried in the air, and stored for the further examinations.

For the preparation of magnetite nanorods, the β-FeOOH powder was homogeneously dispersed in 30 ml DI water and then the suspension was mixed with 150 µl of hydrazine aqueous solution. Afterward, the tube was sealed and placed in the oven, and heated for 4 h at 80 °C. The solution color changed from yellow to black throughout the reaction. The black product was collected magnetically, washed by deionized water multiple times, and dried at 40 °C.

Surface functionalization of magnetite nanorods with APTES

The magnetite nanorods were then surface-functionalized by forming terminal amine groups on their surface using APTES. The as-prepared magnetite nanorods powder (0.2 gr) were mixed with 50 ml APTES solution (12 mM) under constant heating and vigorous mechanical stirring at 80 °C for 1 h. The amine grafted magnetite nanorods were subsequently cooled to room temperature and washed with at least 7 cycles of magnetically collecting and re-dispersion in absolute ethanol/ distilled water solution to remove any residual reactant.

Seeding of magnetite nanorods with gold hydroxide nanoparticle

In the next step, the amine grafted magnetite nanorods were seeded with $Au(OH)_3$ nanoparticles on the surface using a deposition-precipitation process. Briefly, 3 ml of 0.1 M NaOH was added to a 6.25 mM solution of $HAuCl_4$ and allowed stirring for 15 min before the solution becomes mild yellowish. The gold hydroxide solution was formed through hydrolysis of $HAuCl_4$ solution that occurred when pH raised to 8 by adding NaOH. Afterward, 1 ml of the amine grafted magnetite nanorods was added to the as-prepared gold hydroxide solution and heated at 70° C for 30 min under vigorous stirring where the mixture color shifted to orange-brown as an indication for successful loading of $Au(OH)_3$ nanoparticle on the amine-grafted magnetite nanorods. The product was then collected magnetically and washed with distilled water at least 5 times.

Growth of gold shell

The deposited $Au(OH)_3$ nanoparticles acted as nucleation sites for the growth of a gold layer on the magnetite nanorods surface. As a general trend, size of the $Au(OH)_3$ nucleation sites were allowed to grow by surplus addition of reduced gold nanoparticles from $HAuCl_4$ solution. The process was followed to coalesce the nanoparticles and to form a monolith layer of gold shell around the magnetite nanorod's core. Throughout the growth process, the pH of $HAuCl_4$ was adjusted to around 10.1 by the addition of 50 mg K_2CO_3 to 2 ml of $HAuCl_4$ (6 mM) which was diluted in 50 ml distilled water. The solution was allowed to stir in the dark overnight at room

temperature to hydrolyze the $HAuCl_4$ solution and obtain a colorless gold hydroxide solution. This solution would be subsequently mentined as k-gold. Then, 50 mg of seeded magnetic nanorods were added to 20 ml of k-gold solution, where 200 µl of formaldehyde (2%) was added. In this step, complex gold hydroxide anions are reduced on the surface of magnetite nanorods and organize an integral gold shell layer. This reduction resulted in color changes in the solution from red to purple depending on the deposited gold shell thickness and degree of completeness. The Au coated magnetite nanoparticles were separated by a magnet and redispered in water.

Characterization

The optical properties of rod-like gold nanoshells were determined using a UV-Vis spectrophotometer (Unico, Uv-2100) in the range of 500-1000 nm.

The FTIR analysis was performed to distinguish functional groups of the magnetite nanorods before and after functionalization(MNRs and MNRs-APTES). The procedure was carried out through the KBr pellet method and in the wavenumber range of 500-4000 cm^{-1} using an FTIR spectrometer (PerkinElmer, Spectrum RXI). The FTIR spectra of the samples were obtained through 32 scans and in a resolution of 4 cm^{-1}.

The particle size and morphology of the magnetic nanorods were determined by a TESCAN Vega3 SEM. At least 100 nanorods in each micrograph were analyzed in diameter and length using Digimizer software.

TEM images were also prepared by a Zeiss EM10C TEM to distinguish the gold nanoshell layer from the magnetite core.

The XRD spectra of the $FeCl_3$ hydrothermal precipitates and reduced precipitates were recorded at ambient temperature using an X-ray diffractometer (PW 1710 BASED Philips, the Netherlands). Samples in powder form were analyzed using monochromatic Cu/Kα irradiations (λ=1.5406 Å) in a two-tetha range of 10° to 80°.

The magnetic properties of magnetite nanorods were investigated using a VSM (Meghnatis. Daghigh Kavir) in the magnetic range of -5 to 5 kOe at room temperature.

RESULTS AND DISCUSSION

Fromation of nanorods

Fe_3O_4 nanorods were synthesized through hydrothermal formation of β-FeOOH and further reduction by hydrazine. The β-FeOOH suspension showed yellow-colored precipitation which was turned into black after reduction by hydrazine solution (Fig. 1a). The hydrazine-reduced suspension

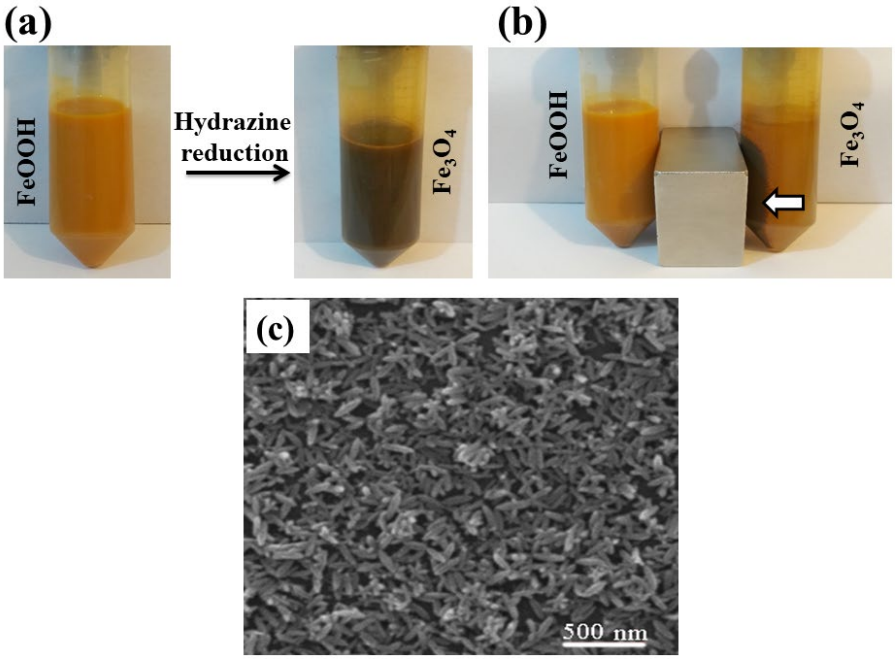

Fig. 1. (a) FeOOH and Fe_3O_4 suspensions, (b) gross magnetic separation of Fe_3O_4 nanorods and (c) SEM images of Fe_3O_4 nanorods 0.05 molar initial concentration of $FeCl_3.6H_2O$

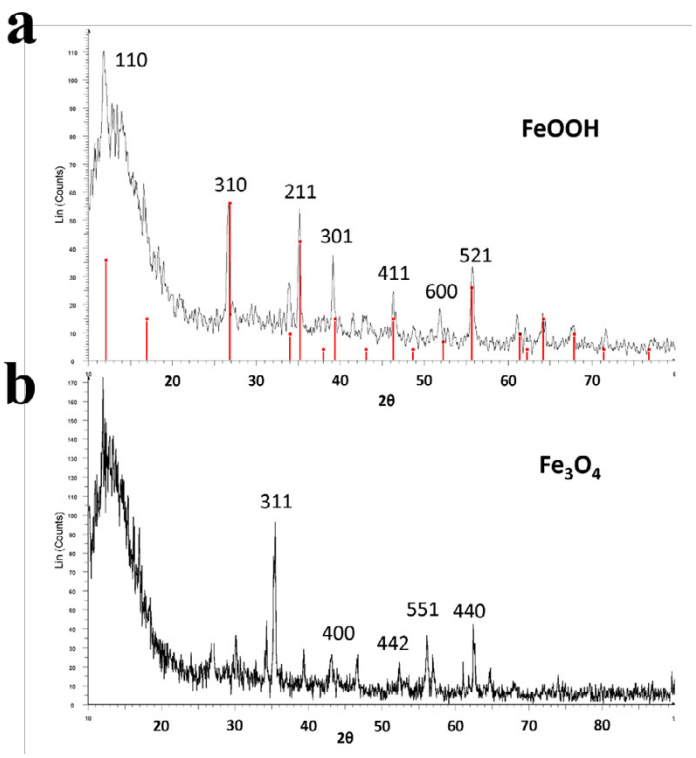

Fig.2. XRD patterns of a) FeOOH and b) Fe_3O_4 nanorods.

was easily capable to be separated through a magnet. This could be an indication for successful formation of iron oxide nanoparticles (Fig. 1b).

The size and morphology of the synthesized magnetite nanorods was investigated by SEM (Fig. 1c). Iron oxide nanoparticles showed a rod-shape morphology with the mean diameter and length of 41.5 ± 7.1 nm and 161.6 ± 26.33 nm nm, respectively. The particles represented rice-like morphology with the aspect ratio of 3.9.

The initial concentration of the precursor is directly in correlation with the mean diameter and average longitude of iron oxide nanorods [33, 34]. Accordingly, the average diameter of magnetite nanorods reduced dramatically when the concentration of Iron (III) chloride, as the precursor, decreased. Additionally, the calculated aspect ratio of obtained nanorods was in the typical range suggested for magnetic nanorods utilized in various biomedical applications including hyperthermia [35-37].

XRD analysis

The crystal structure of the precipitates was characterized using the XRD technique. XRD analysis could be a confirming factor for the successful reduction of the FeOOH nanoparticles and forming the magnetite nanoparticles. The XRD patterns of FeOOH and Fe_3O_4 magnetic nanoparticles are presented in Fig. 2. FeOOH sample showed peaks at 2θ of 11.8°, 16.8°, 26.7°, 35.1°, 39.4°, 46.2°, and 55.9° which were assigned to (110), (200), (310), (211), (301), (401), and (521) crystal planes, respectively. This pattern could be the standard pattern of β-FeOOH nanorods [38-40] that is in agreement with the JCPDS card No. 34-1266.

The peak positions and relative intensities changed after the reduction of FeOOH nanoparticles using hydrazine. The reduced particles showed diffraction peaks at 2θ of 30.1°, 35.5°, 43.3°, 52.9°, 57°, and 62.8° that can be ascribed to (220), (311), (400), (422), (511), and (440) crystal planes of magnetite, respectively. This XRD pattern is in line with the magnetite standard card (JCPDS card No. 19-0629). These alterations in the peak position and relative intensities can be a confirming factor for full conversion of the nanorods from the FeOOH phase to the Fe_3O_4 phase [41, 42].

VSM analysis

Magnetic properties of iron oxide nanorods were examined at room temperature. As can be

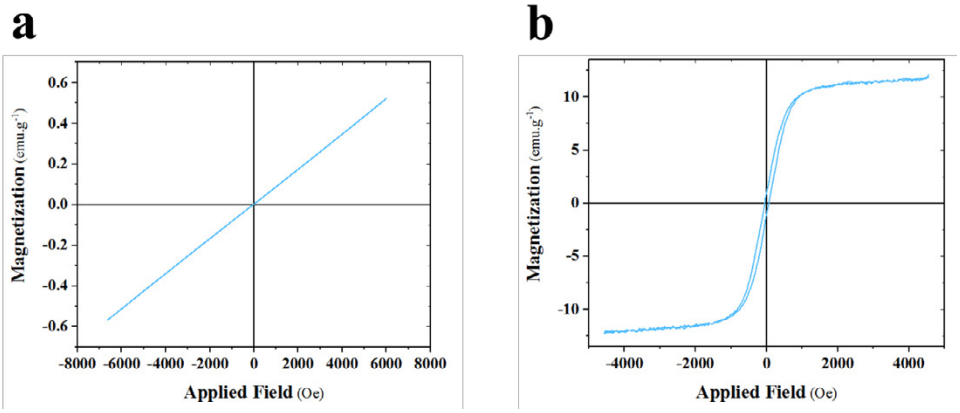

Fig. 3. Magnetization curve of a) FeOOH and b) Fe_3O_4 nanorods.

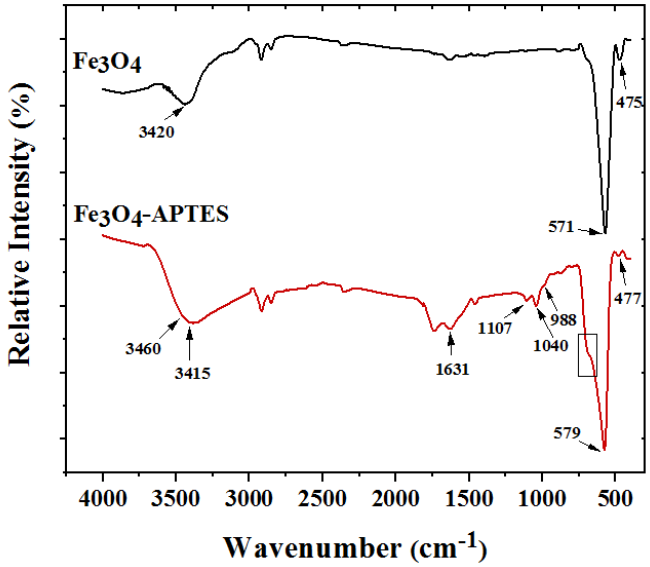

Fig. 4. FT-IR spectra of APTES-coated and Fe_3O_4 magnetite nanorods.

seen in Fig. 3a, the hysteresis curve of the FeOOH nanorods showed a paramagnetic behavior with a saturation magnetization of 0.53 emu/g. On the contrary, the Fe_3O_4 nanorods represented a ferrimagnetic behavior with a small coercivity and remanence (coercivity of 59 Oe and remanence of 0.4 emu/g), along with a saturation magnetization of about 11.71 emu/g (Fig. 3b). The VSM results confirmed the successful reduction of the rod-like FeOOH nanoparticles to the Fe_3O_4 nanorods.

The saturation magnetization of the Fe_3O_4 nanorods is lower than that of the bulk Fe_3O_4. The saturation magnetization of bulk Fe_3O_4 is 89 emu/g. The lower saturation magnetization of the Fe_3O_4 nanorods is due to the disordered surface microstructures or the tiny surface uncompensated spins[43]. The shape anisotropy can also affect the magnetic properties. The Fe_3O_4 nanorods with random orientation could possess different easy magnetic axes magnetizing in different directions. Therefore, the low M_s value could be attributed to the non-collinear spins present on the surface of the nanorods. Furthermore, surface defects can act as pinning centers for the magnetic domains and lead to more decrease in M_s value[38].

FT-IR

The surface chemical structure of bare Fe_3O_4 and Fe_3O_4-APTES magnetic nanorods was characterized by FTIR spectroscopy (Fig. 4). FTIR analysis was utilized to investigate the successful functionalization of Fe_3O_4 nanorods through

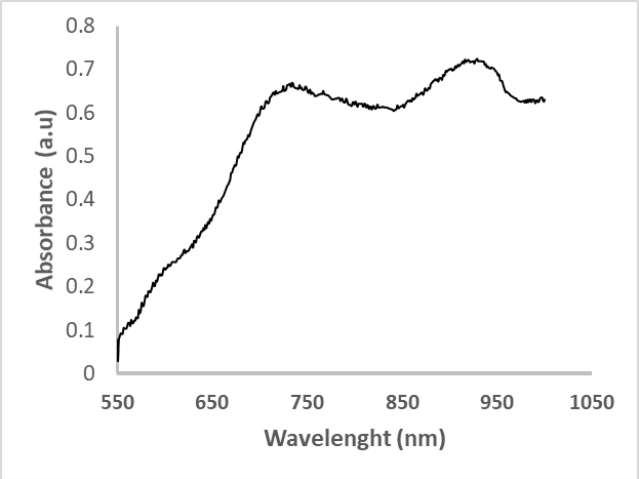

Fig. 5. UV-Vis-NIR Spectra of the rod-shaped gold nanoshells

coating by APTES compound. In the case of bare and APTES-functionalized Fe_3O_4 nanorods spectra, strong Fe–O characteristic peaks appeared at 571 cm^{-1} and 579 cm^{-1} [44]. Shifting of Fe–O characteristic peak to a higher wavenumber in the Fe_3O_4-APTES spectrum might be assigned to the potentially formed interactions between magnetite core and amino-propyl groups. Moreover, an adsorption band around 475 cm^{-1} has emerged in both samples that could be attributed to Fe–O vibrations [45]. These characteristic peaks can be considered as an approval for the existence of the magnetite core of nanorods. Besides, the Fe_3O_4 sample represented a stretching vibration, centered at 3420 cm^{-1}, which corresponds to the vibration band of surface-absorbed O–H groups [46].

However, some newly-emerged peaks could be distinguished in the FTIR spectrum of the APTES-magnetite nanorods. Stretching bands centered at 988, 1040, and 1107 cm^{-1} could be attributed to the Si-O-Si and Si-OH groups of binding APTES molecules [45, 47]. The absorbed silica network (Fe-O-Si bonds), which typically emerged around 584 cm^{-1}, could not be distinguished because of overlapping with the Fe–O characteristic peak (indicated through the rectangular area) [48, 49]. The adsorption band around 3460 could be also attributed to the hydrogen-bonded silanols [50]. Additionally, N-H stretching vibrations (1631 cm^{-1}) and bending of free-NH_2 group (3415 cm^{-1}) can be assigned to the presence of amino-propyl groups on the magnetite surface that is a supplemental confirmation for the successful adsorption of APTES molecules [46, 51].

Optical Properties

Optical properties of the Au coated Fe_3O_4 nanorods with two different gold loading ratios were investigated via UV-Vis-NIR spectroscopy. It is well known that rod-like gold nanostructures exhibit two maximum plasmon resonance absorbance peaks in their UV-Vis-NIR spectra [14]. As indicated in Fig. 5, the prepared Au nanorode showed two separate plasmon absorbance peaks. The observed peaks in Fig. 5 are evidence for the successful forming of the rod-shaped gold nanoshells on the magnetite nanorods. As a general trend, two maximum plasmon resonance absorbance peaks were appeared at around 723 and 924 nm. The absorbance peak at 723 nm could be attributed to the transverse localized plasmon resonances of the rod-shaped nanoshells. The absorbance at 924 nm corresponds to the longitudinal band position of the Au-coated magnetite nanorods [52].

Since both SPR peaks are in the transmission window for biological entities such as skin tissue and hemoglobin, the Fe_3O_4 nanorod/ Au nanoshell platform possesses great potential for in-vivo imaging/ treatment applications.

Transmission Electron Microscopy

The successful formation of a gold nanoshell layer on the surface of magnetite nanoparticles can be studied through transmission electron microscopy. The morphological feature of the Au-coated Fe_3O_4 nanorods was evaluated by TEM. As represented in Fig 6, magnetite nanorods preserved their rod-shaped morphology after the coating by gold layer. Additionally, TEM images indicated a

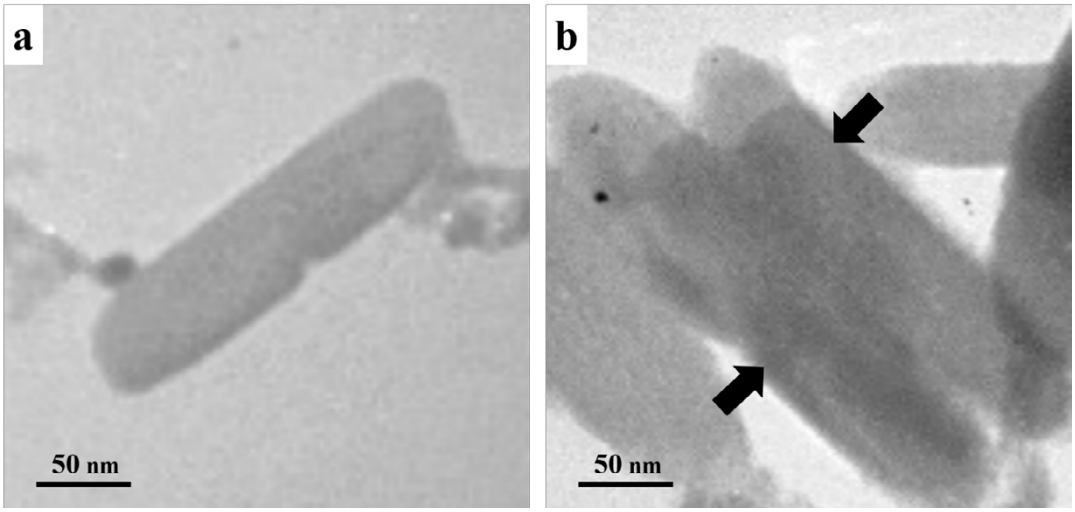

Fig. 6. TEM images of the bare magnetite nanorods (a) and magnetite nanorods coated by Au nanoshell (b).

total coverage of gold shell on the surface of the magnetic nanorods with no distinct fragmentation between magnetite core and gold nanoshell layer. The average diameter of the Au-coated nanorods was calculated 50 ± 7.6 nm that was slightly higher than that of the bare magnetite nanorods (47.1 ± 6.9 nm). This increment might be in line with the formation of the gold nanoshell on the surface. The obtained size and morphology of the synthesized nanorods from the TEM micrographs are in agreement with the findings from SEM images.

CONCLUSION

Gold nanoshells are superior candidates for localized photothermal therapy applications owing to the creating surface heat flux upon NIR light absorption as a consequence of their strong surface plasmon. In this paper, a versatile theranostic platform has been represented through the coating of the magnetite nanorod core via a rod-shaped gold nanoshell layer. This platform might be a potentially considerable candidate for targeted drug delivery, biomedical imaging, and hyperthermia applications. The Fe_3O_4 core was obtained from hydrazine reduction of the rode-like FeOOH particles which has been synthesized through a facile hydrothermal method. The Fe_3O_4 core was then modified with APTES, underwent Au seeding and plating to organize the final gold nanoshell layer. The formation of magnetite nanorods, as the core substrate, was confirmed through SEM, XRD, and VSM analysis. The as-synthesized magnetite nanorods had an aspect ratio of 3.9 with an average diameter of 41.5 ± 7.1 nm. Before the Au coating, successful surface functionalization of the magnetite nanorods by APTES was evaluated and verified using FT-IR analysis. The Au-coated magnetite particles showed two broad plasmon peaks around 723 and 924 nm in UV-Vis-NIR spectroscopy that was confirmation for the formation of a rod-shaped gold nanoshell structure. Additionally, TEM observations further confirmed the homogeneous arrangement of the gold nanoshell layer. All findings suggested that the Fe_3O_4 nanorod/Au nanoshell is a desirable candidate for targeted drug delivery, in-vivo imaging, and photothermal therapy applications.

ACKNOWLEDGEMENTS

This project was financially supported by Shiraz University of Medical Sciences (SUMS), Shiraz, Iran. (Grant No. 1396-01-74-14058).

CONFLICT OF INTEREST

The authors declare no conflicts of interest

REFERENCES

1. Jain PK, Huang X, El-Sayed IH, El-Sayed MA. Review of some interesting surface plasmon resonance-enhanced properties of noble metal nanoparticles and their applications to biosystems. Plasmonics, 2007;2 (3):107-118.
2. Kim M, Lee JH, Nam JM. Plasmonic photothermal nanoparticles for biomedical applications. Advanced Science, 2019;6 (17):1900471.
3. Liu W, Oulton RF, Kivshar YS. Geometric interpretations

for resonances of plasmonic nanoparticles. Scientific reports, 2015;5 (1):1-11.
4. Petryayeva E, Krull UJ. Localized surface plasmon resonance: Nanostructures, bioassays and biosensing—A review. Analytica chimica acta, 2011;706 (1):8-24.
5. Starowicz Z, Wojnarowska-Nowak R, Ozga P, Sheregii E. The tuning of the plasmon resonance of the metal nanoparticles in terms of the SERS effect. Colloid and polymer science, 2018;296 (6):1029-1037.
6. Hao E, Li S, Bailey RC, Zou S, Schatz GC, Hupp JT. Optical properties of metal nanoshells. The Journal of Physical Chemistry B, 2004;108 (4):1224-1229.
7. Kooij ES, Poelsema B. Shape and size effects in the optical properties of metallic nanorods. Physical Chemistry Chemical Physics, 2006;8 (28):3349-3357.
8. Smitha S, Gopchandran K, Smijesh N, Philip R. Size-dependent optical properties of Au nanorods. Progress in Natural Science: Materials International, 2013;23 (1):36-43.
9. Ji X, Shao R, Elliott AM, Stafford RJ, Esparza-Coss E, Bankson JA, Liang G, Luo Z-P, Park K, Markert JT. Bifunctional gold nanoshells with a superparamagnetic iron oxide– silica core suitable for both MR imaging and photothermal therapy. The Journal of Physical Chemistry C, 2007;111 (17):6245-6251.
10. Lévy R, Shaheen U, Cesbron Y, Sée V. Gold nanoparticles delivery in mammalian live cells: a critical review. Nano Reviews, 2010;1 (1):4889.
11. Meng L, Zhang J, Li H, Zhao W, Zhao T. Preparation and Progress in Application of Gold Nanorods. Journal of Nanomaterials, 2019;2019.
12. Chen H, Shao L, Li Q, Wang J. Gold nanorods and their plasmonic properties. Chemical Society Reviews, 2013;42 (7):2679-2724.
13. Hu M, Chen J, Li Z-Y, Au L, Hartland GV, Li X, Marquez M, Xia Y. Gold nanostructures: engineering their plasmonic properties for biomedical applications. Chemical Society Reviews, 2006;35 (11):1084-1094.
14. Shi W, Casas J, Venkataramasubramani M, Tang L. Synthesis and Characterization of gold nanoparticles with Plasmon absorbance wavelength tunable from Visible to Near Infrared Region. International Scholarly Research Notices, 2012;2012.
15. Chapagain P, Guisbiers G, Kusper M, Geoffrion LD, Benamara M, Golden A, Bachri A, Hewavitharana L. Tuning the Surface Plasmon Resonance of Gold Dumbbell Nanorods. ACS Omega, 2021.
16. Bao Z, Liu X, Liu Y, Liu H, Zhao K. Near-infrared light-responsive inorganic nanomaterials for photothermal therapy. asian journal of pharmaceutical sciences, 2016;11 (3):349-364.
17. Wang S, Lin Q, Xu W, An Q, Zhou R, Yu C-J, Xu D, Yuan Z. Precisely tuning the longitudinal localized surface plasmon resonance of gold nanorods via additive-regulated overgrowth. RSC Advances, 2020;10 (21):12619-12625.
18. Pham T, Jackson JB, Halas NJ, Lee TR. Preparation and characterization of gold nanoshells coated with self-assembled monolayers. Langmuir, 2002;18 (12):4915-4920.
19. Wang Y-C, Rhéaume É, Lesage F, Kakkar A. Synthetic methodologies to gold nanoshells: an overview. Molecules, 2018;23 (11):2851.
20. Ye Y, Chen T, Liu Z, Yuan X. Effect of surface scattering of electrons on ratios of optical absorption and scattering to extinction of gold nanoshell. Nanoscale research letters, 2018;13 (1):1-11.
21. Prevo BG, Esakoff SA, Mikhailovsky A, Zasadzinski JA. Scalable routes to gold nanoshells with tunable sizes and response to near-infrared pulsed-laser irradiation. Small, 2008;4 (8):1183-1195.
22. Lien NTH, Duong VTT, Duong V, Hoa DQ, Nhung TH. Theranostic Gold Nanoshells: from Synthesis to Imaging and Photothermal Therapy Applications. Communications in Physics, 2014;24 (3S2):63-70.
23. Oldenburg S, Averitt R, Westcott S, Halas N. Nanoengineering of optical resonances. Chemical Physics Letters, 1998;288 (2-4):243-247.
24. Loo C, Lowery A, Halas N, West J, Drezek R. Immunotargeted nanoshells for integrated cancer imaging and therapy. Nano Letters, 2005;5 (4):709-711.
25. Vatta LL, Sanderson RD, Koch KR. Magnetic nanoparticles: Properties and potential applications. Pure and applied chemistry, 2006;78 (9):1793-1801.
26. Akbarzadeh A, Samiei M, Davaran S. Magnetic nanoparticles: preparation, physical properties, and applications in biomedicine. Nanoscale research letters, 2012;7 (1):1-13.
27. Espinosa A, Bugnet M, Radtke G, Neveu S, Botton GA, Wilhelm C, Abou-Hassan A. Can magneto-plasmonic nanohybrids efficiently combine photothermia with magnetic hyperthermia? Nanoscale, 2015;7 (45):18872-18877.
28. Kumar CS, Mohammad F. Magnetic nanomaterials for hyperthermia-based therapy and controlled drug delivery. Advanced drug delivery reviews, 2011;63 (9):789-808.
29. Quinto CA, Mohindra P, Tong S, Bao G. Multifunctional superparamagnetic iron oxide nanoparticles for combined chemotherapy and hyperthermia cancer treatment. Nanoscale, 2015;7 (29):12728-12736.
30. Xu Z, Hou Y, Sun S. Magnetic core/shell Fe3O4/Au and Fe3O4/Au/Ag nanoparticles with tunable plasmonic properties. Journal of the American Chemical Society, 2007;129 (28):8698-8699.
31. Luchini A, Vitiello G, Rossi F, De Ballesteros OR, Radulescu A, D'Errico G, Montesarchio D, de Julián Fernández C, Paduano L. Developing functionalized Fe 3 O 4–Au nanoparticles: a physico-chemical insight. Physical Chemistry Chemical Physics, 2015;17 (8):6087-6097.
32. Yue J, Jiang X, Yu A. Experimental and theoretical study on the β-FeOOH nanorods: growth and conversion. Journal of Nanoparticle Research, 2011;13 (9):3961-3974.
33. Dehsari HS, Ribeiro AH, Ersöz B, Tremel W, Jakob G, Asadi K. Effect of precursor concentration on size evolution of iron oxide nanoparticles. CrystEngComm, 2017;19 (44):6694-6702.
34. Ghassan AA, Mijan N-A, Taufiq-Yap YH. Nanomaterials: an overview of nanorods synthesis and optimization. Nanorods and Nanocomposites, 2020:11.
35. Fratila RM, Rivera-Fernández S, Jesús M. Shape matters: synthesis and biomedical applications of high aspect ratio magnetic nanomaterials. Nanoscale, 2015;7 (18):8233-8260.
36. Murphy CJ, Jana NR. Controlling the aspect ratio of inorganic nanorods and nanowires. Advanced Materials, 2002;14 (1):80-82.
37. Zhao S, Hao N, Zhang JX, Hoopes PJ, Shubitidze F, Chen Z. Fabrication of monodisperse magnetic nanorods for improving hyperthermia efficacy. Journal of Nanobiotechnology, 2021;19 (1):1-13.

38. Adhikari M, Echeverria E, Risica G, McIlroy DN, Nippe M, Vasquez Y. Synthesis of Magnetite Nanorods from the Reduction of Iron Oxy-Hydroxide with Hydrazine. ACS Omega, 2020;5 (35):22440-22448.
39. Mohapatra J, Mitra A, Tyagi H, Bahadur D, Aslam M. Iron oxide nanorods as high-performance magnetic resonance imaging contrast agents. Nanoscale, 2015;7 (20):9174-9184.
40. Park G, Kim Y-I, Kim YH, Park M, Jang KY, Song H, Nam KM. Preparation and phase transition of FeOOH nanorods: strain effects on catalytic water oxidation. Nanoscale, 2017;9 (14):4751-4758.
41. Chaki S, Malek TJ, Chaudhary M, Tailor J, Deshpande M. Magnetite Fe3O4 nanoparticles synthesis by wet chemical reduction and their characterization. Advances in Natural Sciences: Nanoscience and Nanotechnology, 2015;6 (3):035009.
42. Jia B, Gao L. Selected-Control Synthesis and the Phase Transition of Fe3O4 and α-FeOOH in Ethanol/Water Media. Journal of the American Ceramic Society, 2006;89 (5):1739-1741.
43. Geng S, Yang H, Ren X, Liu Y, He S, Zhou J, Su N, Li Y, Xu C, Zhang X, Cheng Z. Anisotropic Magnetite Nanorods for Enhanced Magnetic Hyperthermia. Chemistry – An Asian Journal, 2016;11 (21):2996-3000.
44. Wang G, Ma Y, Tong Y, Dong X. Synthesis, characterization and magnetorheological study of 3-aminopropyltriethoxysilane-modified Fe3O4 nanoparticles. Smart Materials and Structures, 2016;25 (3):035028.
45. Yamaura M, Camilo R, Sampaio L, Macedo M, Nakamura M, Toma H. Preparation and characterization of (3-aminopropyl) triethoxysilane-coated magnetite nanoparticles. Journal of Magnetism and Magnetic Materials, 2004;279 (2-3):210-217.
46. Saif B, Wang C, Chuan D, Shuang S. Synthesis and characterization of Fe 3 O 4 coated on APTES as carriers for morin-anticancer drug. Journal of Biomaterials and Nanobiotechnology, 2015;6 (04):267.
47. Asab G, Zereffa EA, Abdo Seghne T. Synthesis of silica-coated fe3o4 nanoparticles by microemulsion method: Characterization and evaluation of antimicrobial activity. International journal of biomaterials, 2020;2020.
48. Bruni S, Cariati F, Casu M, Lai A, Musinu A, Piccaluga G, Solinas S. IR and NMR study of nanoparticle-support interactions in a Fe2O3-SiO2 nanocomposite prepared by a sol-gel method. Nanostructured Materials, 1999;11 (5):573-586.
49. Guang-She L, Li-Ping L, Smith Jr R, Inomata H. Characterization of the dispersion process for NiFe2O4 nanocrystals in a silica matrix with infrared spectroscopy and electron paramagnetic resonance. Journal of Molecular Structure, 2001;560 (1-3):87-93.
50. Ramesh S, Felner I, Koltypin Y, Gedanken A. Reaction pathways at the iron-microspherical silica interface: Mechanistic aspects of the formation of target iron oxide phases. Journal of Materials Research, 2000;15 (4):944-950.
51. Xu Z, Liu Q, Finch J. Silanation and stability of 3-aminopropyl triethoxy silane on nanosized superparamagnetic particles: I. Direct silanation. Applied Surface Science, 1997;120 (3-4):269-278.
52. Huang X, El-Sayed MA. Gold nanoparticles: Optical properties and implementations in cancer diagnosis and photothermal therapy. Journal of advanced research, 2010;1 (1):13-28.